Scattered migrating colony formation in the filamentous cyanobacterium, Pseudanabaena sp. NIES-4403

Hiroki Yamamoto
Waseda Daigaku
Yuki Fukasawa
Waseda Daigaku
Yu Shoji
Waseda Daigaku
Shumpei Hisamoto
Waseda Daigaku
Tomohiro Kikuchi
Waseda Daigaku
Atsuko Takamatsu
Waseda Daigaku
Hideo Iwasaki (hideo-iwasaki@waseda.jp)
Waseda University https://orcid.org/0000-0002-3754-4955

Research article

Keywords: Cyanobacteria, Colony pattern formation, Collective behavior, Cell motility

Posted Date: August 19th, 2020

DOI: https://doi.org/10.21203/rs.3.rs-58148/v1

Version of Record: A version of this preprint was published at BMC Microbiology on August 16th, 2021.
See the published version at https://doi.org/10.1186/s12866-021-02183-5.

Scattered migrating colony formation in the filamentous cyanobacterium, *Pseudanabaena* sp. NIES-4403

Hiroki Yamamoto, Yuki Fukasawa, Yu Shoji, Shumpei Hisamoto, Tomohiro Kikuchi, Atsuko Takamatsu, Hideo Iwasaki*

Department of Electrical Engineering and Bioscience, Waseda University, Shinjuku, Tokyo 162-8480, Japan

*Correspondence author

Email addresses:
HY: korigmg@gmail.com
YF: yuki.f.bc@gmail.com
YS: yushog@gmail.com
SH: shumpei.hisamoto.l@gmail.com
TK: 1174970@gmail.com
AT: atsuko_ta@waseda.jp
HI: hideo-iwasaki@waseda.jp

Abstract

Background

Bacteria have been reported to exhibit complicated morphological colony patterns on solid media, depending on intracellular, and extracellular factors such as motility, cell propagation, and cell-cell interaction. We isolated the filamentous cyanobacterium, *Pseudanabaena* sp. NIES-4403 (*Pseudanabaena*, hereafter), that forms scattered (discrete) migrating colonies on solid media. While the scattered colony pattern has been observed in some bacterial species, the mechanism underlying such a pattern still remains obscure.

Results

We studied the morphology of *Pseudanabaena* migrating collectively and found that this species forms randomly scattered clusters varying in size and further consists of a mixture of comet-like wandering clusters and rotating disks. Quantitative analysis of the formation of these wandering and rotating clusters showed that bacterial filaments tend to follow trajectories of previously migrating filaments at velocities that are dependent on filament length. Collisions between filaments occurred without crossing paths, which enhanced their nematic alignments, giving rise to bundle-like colonies. As cells increased and bundles aggregated, comet-like wandering clusters developed. The direction and velocity of the movement of cells in comet-like wandering clusters were highly coordinated. When the wandering clusters entered into a circular orbit, they turned into rotating disks, maintaining a more stable location. Disks may rotate for days, and the speed of cells within a rotating disk increases from the center to the outmost part of the disk. Using a minimal

agent-based model, we reproduced some features of *Pseudanabaena* migrating clusters.

Conclusion

Based on these observations, we propose that *Pseudanabaena* forms scattered migrating colonies that undergo a series of transitions involving several morphological patterns. A minimal agent-based model is able to reconstruct some features of the observed migrating clusters.

Keywords: Cyanobacteria, Colony pattern formation, Collective behavior, Cell motility

Background

Bacterial colonies are formed through biological self-organization [1-10]. For example, pioneering studies on the morphology of *Bacillus subtilis* colonies demonstrated that colony morphology depends on the solidity and nutrient concentrations of the media [3, 11]. These results have been simulated numerically [4, 12].

Self-propelled bacteria often show complicated collective behaviors, such as the formation of dense moving clusters, which is exemplified by "wandering" (comet-like) and "rotating" colonies as described by Henriksen[6, 13, 14]. These colony patterns have been analyzed in detail, mainly in *Bacillus circulans* and *Paenibacillaceae*. For example, *Paenibacillus vortex* forms both wandering and rotating clusters when cells elongate in the presence of mitomycin C [7] or when they are co-cultivated with *E.coli* [15]. *Paenibacillus alvei* also forms wandering colonies [16], while *Paenibacillus* sp. NAIST15-1 forms both wandering and rotating colonies [8]. Meanwhile, *Myxococcus xanthus* is a bacterium that forms large moving clusters such as vortices, bundled circular patterns, side-by-side clusters, and rafts [17, 18]. In this species, EPS associated with the pilus [19, 20] and its trail [21] and its ability to reverse directions [18, 22] have been suggested to contribute to cluster formation via cell-cell interaction.

Motile cell aggregates have also been observed in cyanobacteria. Some filamentous cyanobacteria often exhibit circular (hollow ring) colony patterns [10, 23, 24, 25]. Like *Bacillus*, the unicellular cyanobacterium, *Synechocystis* sp. PCC 6803 is known to form finger-like expanding clusters that are probably important in phototaxis and slime secretion [26, 27, 28, 29]. The comet-like wandering aggregate has been described in *Pseudanabaena galeata* [30, 31], a phototactic cyanobacterium. It should be noted that cyanobacteria lack flagella, an appendage used in collective behaviors of *Bacillus* and *Paenibacillus* to form a similar type of aggregate [32, 33]. Thus, the mechanism behind such colony morphologies are likely due to some shared means of self-organization, regardless of the type of molecular machinery used for gliding. However, previous reviews on *Pseudanabaena* by Castenholz (1982, 2001) have devoted only a few paragraphs regarding this issue; thus, detailed information is not available.

Here, we report the isolation of *Pseudanabaena* sp. NIES-4403, a filamentous cyanobacterium that forms both comet-like wandering aggregates and rotating clusters on solid media. At the macroscopic level, the mixture of wandering, and rotating clusters forms randomly scattered clusters that vary in size. We investigated these clusters microscopically and performed quantitative analyses on the formation and motility of these clusters and on the temporal dynamics of the scattered pattern. Mathematical modeling was also employed to reproduce the development of the scattered pattern.

Results and Discussion

Scattered patterning of *Pseudanabaena* colonies

We isolated a filamentous cyanobacterium (**Figs. 1a–c**) from a pond at Waseda University in Tokyo (35.706008, 139.707843). The cyanobacterium displayed remarkable colony morphology on solid media. Phylogenetic analysis of its16S rRNA gene has revealed that this strain is closely related to the genus

Pseudanabaena (**Fig. S1**). Thus, we registered this strain as *Pseudanabaena* sp. NIES-4403 at the Microbial Culture Collection of the National Institute for Environmental Studies (NIES collection). On BG-11 solid medium, this cyanobacterium was observed to develop randomly scattered clusters that varied in size (**Fig. 1d**). When a cell suspension was placed at the center of agar plates, growing cells glided on the surface and showed a series of dynamic collective behaviors (**Fig. 2a, Movie S1**). One collective behavior gives rise to comet-like clusters, and these occasionally form vortices called "rotating disks." These disks may reach a diameter of ~1 mm (see below).

The randomly scattered pattern on solid media (**Fig. 1d, Fig. 2a**) looks similar to the "stellar" pattern that has been briefly described in *Paenibacillus alvei* [34] (we prefer to call "starry-like", though) and whose mechanism of formation remains unknown. Approximately one day after cells were inoculated at the center of the solid media (**Fig. 2a** left, hour 0 in **Movie S1**), highly dense, moving (comet-like) clusters started spreading and traveled around (**Fig. 2a** middle and right, hours 100 and 200 in **Movie S1**). Some of the clusters became organized into small circular orbits that sometimes coalesced when the head and tails of clusters attached, thus developing into a rotating disk. Most of the rotating disk kept rotating as the cells grew (**Fig. 2b** for passing count imaging), although a minor fraction of the cell population reverted back to comet-like clusters that travel throughout the surface of the medium (see below). A kymograph shown in **Fig. 2c** represents a time-dependent profile of bacterial cluster formation and its transitions. Transiently appearing patterns of dark dots and sloped short bars (cyan arrowhead) on the kymograph indicate the passage of wandering comet-like clusters, while vertical gradient lines (magenta arrowhead) represent rotating clusters that remain in one location and gradually expands in size. Details of this will be discussed later. Interestingly, the probability distribution function (PDF) of cluster size distributions (including comet-like clusters and disks) follows a roughly straight line on a log-log plot, regardless of time after inoculation (hour 100 or 200 in **Fig. 2d**). This distribution is reminiscent of random multiplication processes that contribute to power-law or log-normal distributions and further underlie the behavior of complex systems in which various elements are connected to various stochastic factors from the past. Thus, the result in **Fig. 2d** suggests that the development and decay of bacterial clusters depend on a history-dependent random multiplication process. To better understand this process, the cumulative distribution function (CDF) of the colony size distribution is presented in **Fig. 2e,** and we tested whether this distribution is similar to either a power-law or log-normal distribution using a method described by Clauset *et al.* [35] implemented within the poweR-law package [36, 37] on R (for details, see Materials and Methods). Clauset *et al*. [35] proposed that the null hypothesis H_0 (the experimental data follows the power-law distribution) may be rejected if the *p*-value is less than 0.1. On the one hand, the *p*-values calculated to determine the degree of fit to the power-law distribution were 0.15 and 0.01 for the experimental data at hours 100 and 200, respectively. On the other hand, the corresponding *p*-values determining fit to the log-normal distribution [35, 36 for details] were 0.12 and 0.89, respectively. We also performed the Vuong's test, which is a likelihood ratio test for model selection using the Kullback-Leibler criterion [35, 36], to determine whether the model distribution is closer to power-law or log-normal. Here, the null hypothesis H_0 (both distributions are equally far from the true distribution) is tested against the alternative hypothesis H_1 (one of the test distributions is

closer to the true distribution). A *p*-value greater than 0.1 indicates that it is difficult to determine which distribution is more appropriate, according to Clauset *et al*. [35]. According to our calculations, the *p*-values for the data at hours 100 and 200 are 1.02E-08 and 1.34E-03, respectively. Taken together, our results suggest that the power-law distribution is a better fit for the experimental data at hour 100, while the log-normal distribution is a better fit for the data at hour 200. This is consistent with our findings for the CDFs for data at hours 100 and 200, in which the former follows a straighter line on a log-log plot, which indicates a power-law distribution (**Fig. 2e**). This suggests that an additive fluctuation effect due to random multiplication processes is more apparent at hour 100, which is possibly due to rapid exponential growth of cells at this stage. Meanwhile, at hour 200, the effect of cell propagation is weakened due to slower growth.

Comet-like wandering clusters

Figure 3a shows a representative trajectory during gliding movement of a comet-like cluster on solid media for ~120 h (for movie, see **Movie S2**, which had been extracted from **Movie S1**). This cluster originated close to the central position (inoculation point) of the plate and then wandered along the route shown by the dotted lines (from cyan to magenta, **Fig. 3a**). During the course of traveling, the area occupied by the cluster almost doubled linearly (**Fig. 3b**, orange line). Clusters grow by (i) integration (unity) of multiple clusters and/or by (ii) cell growth. We then analyzed the growth of a cluster on **Figs. 3a–b**, wherein the size was determined to expand even when it wandered at peripheral positions of the plate where visible colonies were not present. This indicates that cells grow within wandering clusters. The cluster moved at a stable velocity of ~ 0.2–0.25 μm/s for most of the experiment. However, transient increases in velocity were observed three times: at hours 154, 177, and 193 (**Fig. 3b**). Interestingly, at hours 177 and 193, the cluster was crossing over positions that it had previously passed. Thus, gliding speed may accelerate due to micro-environmental changes elicited by previously passing bacterial colonies. For example, a passing cluster may change the water environment on the solid surface by secreting mucilage, as discussed below. Notably, in *Paenibacillus* sp. NAIST15-1, an extracellular protein CmoA may play a role in wandering and rotating clusters by affecting water uptake from the agar medium [8]. The transient increase in cluster velocity at hour 154 did not occur at a location that it had previously passed; however, at least three other comet-like clusters had previously passed this position (**Fig. 3c**). We suggest that the trails of these clusters affected the acceleration of the cluster we were monitoring due to the same reason that explains the accelerations at hours 178 and 195.

The stability of comet-like clusters (for better resolution, see **Fig. 3d** and **Movie S3**) suggests a tight interaction among bacterial filaments. To determine the detailed architecture of a cluster, we observed its surface structure by confocal microscopic analysis (**Fig. 3e, Movie S4**). The cluster moved at a rate of approximately 100 μm within 590 s, without changing the relative positions of cells within the cluster, as indicated by particle image velocimetry (PIV) analysis (**Fig. 3e**). Some exceptions consisted of filaments near the head of the structure that did not bind tightly to the cluster. Matsuyama and Matsushita [35] reported that *Bacillus subtilis* has formed finger-shaped extending branches in which cells at the outermost tip wall remain immotile, while the inner cells randomly swirl, pushing the tip wall cells to extend the branch

(division of labor). The tip wall of the comet-like wandering cluster in *Pseudanabaena* is also covered by layers of filaments that can be pushed by inner filaments that are aligned along the axis of the cluster. However, unlike *Bacillus subtilis*, the relative positions between the tip wall filaments and the inner nematically aligned filaments change little as the cluster moves (**Movie S4**). In *Pseudanabaena*, it is still unclear if the wall tip cell layer moves passively by being pushed by the following aligned filaments or by self-propelled, active motive force. It should be noted that even U- or horseshoe-shaped single filaments are able to move autonomously (**Fig. 3f**). Cells on the bottom side of a cluster are stably attached to the solid agar surface, which means that the filaments in the upper layers, horizontally situated above the bottom side, do not directly associate with the agar surface. Therefore, another type of division of labor must be involved in wandering clusters in *Pseudanabaena*. In this case, the bottom side filaments appear to be more responsible for driving motility, while cells in the upper layers do not move. As the cluster becomes larger, it expands both two-dimensionally and along the Z-axis. Thus, if cells in the upper layers do not contribute to motility, then the speed of gliding movement should decrease. However, this slowing down was not observed. Therefore, we suggest that filaments in the upper layers also contribute somewhat to cluster motility (see below).

Rotating disk

Figure 4a shows a representative trajectory of gliding movement for ~40 h on solid medium by a comet-like cluster that was the process of turning into a rotating disk (see also **Movie S5**). The cluster originated from the center of the plate at hour 22 and then wandered along the route shown by the dotted lines (from cyan to magenta, **Fig. 4a**). Thereafter, the cluster transformed to form a compact circular orbit, resulting in a transition from the comet-like wandering colony to the rotating disk at around hour 56. The size of the cluster decreased slightly during the transition into a disk (hour 56), which also occurred as a comet-like cluster (**Fig. 3b**). However, the size was observed to increase linearly after hour 61 (**Fig. 4b**, red line). Although the rotating disk appears to stay in place (**Fig. 4b**, blue line), this does not mean that cells in the rotating disk do not move. As mentioned earlier briefly, at the cellular scale, filaments within a rotating disk maintain a circular motion (**Fig. 4c**, **Movie S3**). We have observed that a large rotating disk with a diameter of ~ 1 mm usually remains at a terminal collective mode; however, it maintains its rotation for more than 10 days. The vertical wavy lines on the kymograph shown in **Fig. 2c** indicate continuous, regular rotation. This is quite different from previously reported rotating clusters in *Paenibacillus* sp. NAIST15-1, which immediately stop rotating after forming large vortices [8]. Such collective aggregate movements also result in a scattered (discrete) colony pattern. In such vortices of bacteria, in general, cells at the edge of a rotating aggregate move faster than cells at the center [2, 36]. This was confirmed in *Pseudanabaena* by PIV analysis of a video of a rotating disk that was recorded through a confocal microscope (**Fig. 4d**, **Movie S6,** and **Fig. S2**). **Figure 4e** shows distribution of velocities, which were measured from the center to the outermost part of the disk. The plots likely consists of three components: (1) a central zone measuring less than ~30 μm (**Fig. 4e**) where very slow or randomly moving filaments are dominant with lower filament density; (2) a rotating zone (~100 to ~180 μm in **Fig. 4e**) where the velocity is elevated

depending on the distance from the center; and (3) a peripheral or outmost zone (~180-220 μm in **Fig. 4e**) that contains a mixture of filaments that move at fast and slow speeds. If a rotating aggregate is perfectly rigid, the rotation speed $v(R) = \omega R$, where R is the distance of the point from the center and ω is angular speed of the rotating disk. Although the distribution of velocity shown in **Fig. 4e** is not perfectly on a straight line, the results confirmed the speed increased depending on the distance from the center. The sudden drop in the velocity at the peripheral/outmost zone can be attributed to the presence of immotile or slowly moving bundles or filaments being dissociated from the rotating cluster (see **Movie S6**).

Bundles and single filaments

Except for the comet-like wandering clusters and rotating disks, most bacterial filaments move alone or form bundles (**Fig. 5a**). A bundle is formed when several filaments align themselves along their longitudinal axis. In comet-like wandering clusters and rotating disks, most of the filaments move in coordination with other nearby filaments. By contrast, filaments in bundles are not always stably aligned, and bundles may often dissolve or merge with each other. For example, **Fig. 5a** shows most of the filaments in the bundle move to the lower side; however, two filaments of the bundle moved to the tip of the bundle at the upper side, resulting in the division of this bundle into three bundles (**Movie S7**). As mentioned above, some filaments may move against the lateral axis to form a U-shape (**Fig. 3f**). In other filaments moving along their longitudinal axis, some may switch or "reverse" their direction of movement. We tended to observe such reversals in movement with dispersed filaments or with relatively free moving filaments at the peripheral region of cellular aggregates, and we rarely observed the phenomenon inside of high-density clusters. As filaments move, they leave behind a kind of trail that other filaments may follow, as if being guided (**Fig. 5b, Movie S8**). Although the details of such trails remain unclear, it is likely that the mechanism depends on either a groove created on the solid surface or on secreted mucilage, such as extracellular polysaccharides (EPS) that are proposed to activate motility in gliding bacteria [40, 22], or both. In any case, the ability to follow trails should facilitate collective behavior [21]. Staining the EPS with Alcian blue has resulted in some faint signals around cells (**Fig. S3**). Thus, it is likely that *Pseudanabaena* cells secrete EPS, although more detailed analysis is necessary to determine if it is involved in trail formation. When two filaments collide, in most cases, the filaments do not cross paths, but instead align with each other to form a bundle (**Fig. 5c**, **Movie S9**). This characteristic, also known as "nematic alignment," has been proposed in *Myxococcus xanthus* [38], and this appears to be a key collective behavior in *Pseudanabaena* as well. It should be noted that in high-density clusters, neighboring filaments are essentially aligned with each other.

The velocity of a single filament gliding on a solid surface without following trails (i.e., moving on a virgin field) ranged from 0.02 to 0.19 μm/s, depending on the filament length (**Fig. 5d**). Below a length of 200 μm, filament velocity appears to be proportional to the length (**Fig.5d**). The correlation is higher at lengths below ~100 μm (**Fig. S4**), which produces a Spearman's rank correlation coefficient of 0.74. The length-velocity correlation has also been reported in *Phormidium* sp. [25], which is another cyanobacterium whose average velocity increases with filament length, which the authors ascribed to the

lowering occurrence of the reversal behavior (in that report, higher velocity represents longer net displacement). By contrast, **Fig. 5d,** showing the relationship between velocity and length of filaments, is based on the velocity of filaments that did not reverse their direction of movement during observation. We were aware that the reversal behavior is more frequently observed for shorter filaments, especially during early development immediately following inoculation. It is possible that each cell has motors that are more effective in longer filaments. In addition, or alternatively, cellular motors may be better synchronized in the longer filaments (up to ~200 μm). Moreover, it is also possible that longer filaments secrete more mucilage, which can reduce friction between the filament and the solid surface. It should be noted that the comet-like wandering colony consists of thousands of filaments, and it moves at a velocity that is comparable or slightly higher than the maximal speed of single filaments (0.19 μm/s). This velocity may increase transiently (up to 0.5 μm/s) when the colony crosses over pre-existing trails (**Figs. 3b** and **3c**). Thus, even though the nematic alignment of thousands of filaments may be expected to facilitate movement and increase velocity to some extent, it likely contributes more to unifying the direction of motion and the speed of each filament.

The mechanism of gliding motility in *Pseudanabaena* remains to be unknown. However, some models have been proposed for other filamentous cyanobacteria. *Oscillatoria* has been proposed to move by distorting proteinaceous fibrils on its cell wall [39, 40]. In *Phormidium uncinatum*, slime secretion from the junction pore complex (JPC) has been proposed to be the driving force behind motility [41]. In differentiated motile hormogonia of *Nostoc punctiforme*, Type IV pili are identified as the means of motility [42]. In this case, molecular analysis has revealed that the Type IV-pilus-like structure is encoded by *pil* and *hps* genes that play roles in motility and polysaccharide secretion [46, 47, 48]. According to Khayatan *et al*. [45], the *pil* and *hps* genes are reportedly conserved in *Pseudanabaena* sp. PCC 7367. Thus, a *Nostoc*-like motility system may underlie the colony patterns observed in the present study. It should be noted, however, that high-density wandering and disk patterns have not been observed in hormogonia of *Nostoc punctiforme*. The mechanism of pattern formation in *Pseudanabaena* should address how filaments associate with each other to coordinate aggregation and motility.

Transition of colony patterns

During the course of cultivation, clusters may change their patterns to any of those previously described (bundle, wandering comet, or rotating disk). When the density of cells/filaments is determined to be relatively low (early after inoculation), single filaments may collide, and align into a bundle as mentioned above. **Figures 6a–f** present a schematic diagram of the possible steps in the development of clusters. We suggest that comet-like wandering colonies develop from top covered bundles, as shown in **Figs. 6a** and **6b**. **Figure 6a** (upper panel) shows a protruding filament at the outer side of a bundle as it spontaneously changes its curvature, while other neighboring bundles move forward, thus pushing the curved filament to form the top cover of the comet precursor. The lower panel of **Fig. 6a** shows that a filament or bundle may collide against a filament perpendicular to the direction of the former, thus forming a comet precursor. This top cover plays an important role in keeping the alignment of filaments stable, enabling them to move

uniformly as an organized wandering cluster, at least at the initial stage. Otherwise, filaments easily dissociate from each other as it is often observed for bundles (i.e., "bundle to single" transition). The top covering filament at the initial stage also works as a trap, collecting bundles, or single filaments that enable the comet precursor to grow.

We propose that the formation of a high-density cluster requires a positive feedback system in order to facilitate aggregation. Comet-like wandering colonies become larger (**Figs. 6b–d**) via both cell propagation and collision-based uptake of bundles or other comets, as shown in **Fig. 6g** and **Movie S10**. Well-developed, comet-like wandering clusters may spontaneously curve due to local differences in velocities of filaments inside the cluster, possibly triggered by friction from the solid surface of agar, or partial attachment with trails (**Fig. 6e**). As a comet-like cluster enters into a circular orbit, it turns into a rotating disk (**Fig. 6h**, **Movie S11**). As mentioned earlier, most of such disks maintain a stable rotation, thus developing into a terminal cluster. Nevertheless, some disks may revert back to comet-like clusters by colliding with another comet-like cluster as shown in **Fig. 6i** and **Movie S12**. On the kymograph shown in **Fig. 2b**, this type of transition is represented by the sudden termination of vertical lines (rotating disks).

Mathematical modeling of the scattered pattern

We employed an agent-based model to reproduce scattered clusters on solid media. The model is based on a recently proposed model reproducing the collective pattern formations in *C. elegans* [46], which itself is derived from a model for the pattern of large vortices of microtubes *in vitro* [50, 51]. The key features of this model are identified as follows: (i) the direction of movement of each particle attains uniformity by nematic order; and (ii) the rotation rate of particles is maintained for a relatively long period, as we have observed in *Pseudanabaena*. The previous model applied for *C. elegans* was run in a torus field to reproduce a small space, and resulted in the formation of a dynamical network and the stabilization of particle movements. By contrast, we ran our modified model in infinite space with locally condensed particles at the initial position to represent the actual inoculation situation (**Fig. 2a**). Under this modified condition, we predict that particles will not form a stable pattern and, in the end, will diffuse into infinite space. Details of the modified model are expressed as:

$$\mathbf{r}_{i,t+1} = \mathbf{r}_{i,t} + v_0 \mathbf{e}_{\theta_{i,t+1}} + v_0 \sum_{r_{ij}<r^r} \mathbf{F}_{ij}^r + \frac{1}{N_i} v_0 \sum_{r^r<r_{ij}<l} \mathbf{F}_{ij}^a \quad \#(1)$$

$$\theta_{i,t+1} = \theta_{i,t} + \omega_{i,t+1} + \frac{1}{N_i} \sum_{r^r<r_{ij}<l} sin2\left(\theta_{j,t} - \theta_{i,t}\right) \quad \#(2)$$

$$\omega_{i,t+1} = \omega_{i,t} - \frac{\omega_{i,t} - \omega_0}{\tau} + \sqrt{\frac{2}{\tau}} \sigma_\omega \xi_i \quad \#(3)$$

$$\mathbf{F}_{ij}^{r} = k^{r}\left(r_{ij} - r^{r}\right)\mathbf{e}_{ij} \#(4)$$

306

$$\mathbf{F}_{ij}^{a} = \frac{k^{a}}{r_{ij}}\mathbf{e}_{ij}, \#(5)$$

307 where $\mathbf{r}_{i,t}$ is the position of a particle *i* at step *t*. The particle *i* then moves to $v_0\mathbf{e}_{\theta_{i,t}}$ at step *t*, where v_0
308 and $\theta_{i,t}$ are the unit velocity and the direction of motion, respectively. $\mathbf{e}_{\theta_{i,t}}$ is the unit vector in the
309 direction of $\theta_{i,t}$, The direction is derived from rotation rate $\omega_{i,t}$ and that of other N_i particles in $r^r < r < l$
310 as an effect of alignment. *l* is the distance of interaction or filament length. The particle also receives
311 attractive force $\mathbf{F}_{ij}^{a}$ ($r^r < r < l$) or repulsive force $\mathbf{F}_{ij}^{r}$ ($r < r^r$) from neighbor particles. Parameters used in
312 our simulation are listed in Table 1.

313 These parameters are essentially the same as those reported in a previous model[46], except the
314 attraction term in equation (1) is divided by particle number N_i in order to avoid excessive increments of
315 attraction under high-density conditions. We employed the newly fitted parameters as summarized in
316 **Table 1** for our simulation, the results of which are presented in **Fig. 7** and **Movie S13**, which correspond
317 to the *in vivo* experimental observations shown in **Fig. 2** and **Movie S1**, respectively. In our simulation,
318 particles have gathered and moved collectively like a comet-like wandering cluster (**Figs. 7a** and **7b**) that
319 the kymograph on **Fig. 7c** represents short, sloped bars. Some of these clusters entered into circular orbits
320 as represented by periodically appearing short, sloped bars aligned to the vertical axis of the kymograph
321 (**Fig. 7c**). The circular orbits of the simulated clusters were found to be transient (**Movie S13**, **Fig. 7c**),
322 similar to comet-like wandering clusters moving tentatively on circular trails. It should be noted that this
323 simple simulation does not implement the effects of mucilage secretion to facilitate trail-following and cell
324 propagation, both of which contribute to change the density and size of aggregates. Nevertheless, the
325 scattered colony patterning in *Pseudanabaena* (**Fig. 2a**) is at least partially reproduced by our model (**Fig.**
326 **7a**) with somewhat similar trajectory profiles (**Figs. 2b** and **7b**). Colony size distribution and the
327 cumulative distribution profiles observed in our experiments (**Figs. 2d** and **2e**) were also reproduced in our
328 simulation (**Figs. 7d** and **7e**), to some extent. We tested whether the cluster sizes generated from empirical
329 data would follow either a power-law or log-normal distribution (**Figure 2e**) but failed to show which is
330 more appropriate; that is, the *p*-values of the Vuong's likelihood tests compare our results to the power-law
331 and log-normal distributions were 0.87 and 0.15 at steps 1000 and 2000, respectively. Nevertheless, our
332 results are consistent with the assumption that a random multiplication process contributes to the formation
333 of scattered colony patterns in *Pseudanabaena*.

334

335 **Conclusion**

336 We describe the morphology of colony pattern formation based on the collective behaviors of the
337 filamentous cyanobacterium, *Pseudanabaena* sp. NIES-4403. Aggregates were determined to develop into
338 randomly scattered clusters varying in size and further consist of a mixture of comet-like wandering clusters
339 and rotating disk-like clusters. Our study suggests that the following processes are key to pattern formation:
340 (1) trail following of filaments possibly through polysaccharide secretion and/or groove formation on the

solid surface, (2) bundle formation with nematic alignments, (3) top covering-induced formation of comet-like wandering clusters, (4) rotating disk formation through spontaneous self-following of the wandering cluster, and (5) collision-based transition among different cluster types. Based on the simple assumptions of nematic interaction and temporal maintenance of the direction of motion, our agent-based model reproduced some characteristics of the scattered colony formation. Although the observed morphologies were observed under artificial conditions, we speculate that these features contribute to the adaptive fitness of this species in its natural environment. For example, the formation of a highly dense cluster without long-distance migration, as exemplified by the rotating disk, should be of advantage in forming a stable biofilm under preferred growth conditions. In addition, the ability to coordinate migration via a comet-like wandering cluster moving at maximal speed should facilitate colony expansion or escape from undesirable condition. In other words, this cyanobacterial species has developed its own strategy to form biofilms that includes some positive feedback-based aggregation and dispersing processes. The morphological patterns produced under pure culture conditions on an artificially flat solid surface are manifestations of a strategy that has evolved under natural conditions. Further analysis should be conducted to compare collective behaviors under more natural conditions and under simple experimental conditions.

Methods

Strains and culture

Pseudanabaena sp. NIES-4403 was isolated on BG-11 solid medium by H.I. from pondwater in the Nishi-Waseda Campus of Waseda University, Tokyo, Japan (north latitude 35.706005, east longitude 139.707850). Cells were cultured on BG-11 medium [49] containing 1.5 % of Bacto^{TM} agar (BD Falcon, USA) under continuous light illuminated by fluorescent lamps (around 30 μmol m^{-2} s^{-1}) at 30 °C. Subculturing was performed every 2 weeks by inoculating 4 μl of cell suspension on fresh BG-11 agar plates.

Phylogenetic tree analysis

A region of the 16S rRNA gene was then amplified by colony PCR using primers 27F (5'-AGAGTTTGATCCTGGCTCAG-3') and 1494R (5'-GTACGGCTACCTTGTTACGAC-3'). The amplified DNA fragment was further cloned into the pGEM-T Easy vector (Promega, USA) and transformed into *E. coli* JM109 cells (Takara Bio, Japan). The PCR-derived segments of the resulting plasmids were sequenced (Applied Biosystems 3730xl, Thermo Fisher, USA) using the same primers, and the resulting sequence was compared to 16S rRNA gene sequences from 29 cyanobacterial species (downloaded from the Ribosomal Database Project (RDP) on Mar 23, 2018)[50]. Twenty-four sequences with higher BLASTn (version 2.2.28+) similarity scores [51], excluding the sequences of "Uncultured Bacterium" and 5 sequences of representative cyanobacterial species (*Synechocystis* sp. PCC 6803, *Nostoc punctiforme* PCC 73102, *Anabaena* sp. PCC 7120, *Anabaena variabilis* ATCC 29413, and *Synechococcus* sp. PCC 7942) were chosen to compare with the sequence derived from *Pseudanabaena*. These 16S rRNA

gene sequences and that of *Pseudanabaena* sp. were aligned with MUSCLE (version 3.8.31)[52], calculated with ClustalW (version 2.1)[53], and used to generate a phylogenetic tree using Archaeopteryx (version 0.972 9m)[54] (Fig. S1).

Imaging of colony patterns

Microscopic images were taken using a CCD camera (RETIGA EXi FAST 1394; QImaging, Canada) coupled to an inverted microscope (IX71; Olympus, Japan) equipped with UPlanFLN (4x) and LUCPlanFLN (20x) objectives (both Olympus). The system was controlled by SlideBook software (Intelligent Imaging Innovations, USA). Confocal microscopic images were taken using the FV-1000D system (Olympus) connected to the IX81 automated microscope (Olympus) equipped with the LUCPlanFLN (20x) objective (Olympus) and controlled by FV10-ASW software. 559 nm laser excitation was used to visualize the autofluorescence from cyanobacterial filaments. For confocal imaging, cells were cultured on BG-11 plates containing 1.5 % of Gelrite (Fujifilm Wako Pure Chemical Corporation, Japan) instead of agar for clarity. We confirmed that the colony patterns produced by *Pseudanabaena* on these plates look essentially the same as those formed on agar plates. All microscopic observations were illuminated by fluorescent lamps (around 30 μmol m^{-2} s^{-1}). Macroscopic images of colonies on 90-mm plates (shown in **Figs. 1d**, **2a**, **3a,** and **4a)** were taken by a single-lens reflex camera (K-5 II, Pentax, Japan). An LED tracing stand (ARTON SMART TRACER PRO A4, Dai-Nippon Bijutu Kougei, Japan) placed underneath the plate was used as a light source (approximately 30 μmol m^{-2} s^{-1}) for both photography and cell culture. A thermo glass plate (Microwarm Plate KM-1/MP-1000H, Kitazato, Japan) set to 33 °C was placed on top of the agar plates to maintain the growth temperature and avoid condensation.

Alcian blue staining of EPS

Twenty microliters of cell suspension was incubated on a slide glass for 30 min. Any floating cells and liquid were removed gently by absorbing to filter paper. The materials remaining on the slide, including the cells, were stained with 20 μl of 1.5 % (w/v) Alcian blue 8GX (Sigma-Aldrich, USA) for 30 min. Then, the Alcian blue solution was replaced by 20 μl of BG-11 liquid medium, and a coverslip was then mounted onto the droplet. Stained materials were observed under the IX-51 microscope with an UplanFLN (10x) objective (Olympus, Japan), and images were collected using the Color CMOS camera, Moticam 5 (Motic, China).

Electron Microscopy

Cells were fixed with 2.5 % glutaraldehyde dissolved in 0.1M phosphate buffer solution at 4 °C, washed with phosphate buffer solution, and additionally fixed with osmium tetroxide at 4 °C. Samples were then dehydrated several times in a 50 % to 100 % ethanol series and then freeze-dried. For SEM observation, dehydrated cells were coated with osmium and observed using a JSM-6320F SEM (JEOL, Japan). For TEM observations, dehydrated cells were embedded in epoxy resin (EPON812; Shell Chemical, USA), and ultrathin slices of the material were doubly stained in uranyl acetate and lead citrate. The sections were coated with carbon in a vacuum vapor deposition system, and then the coated ultrathin slices of cells were

observed using TEM (JEM1200EX, JEOL). All observations were performed at the Hanaichi UltraStructure Research Institute (Okazaki, Japan).

Image processing

Images were processed and analyzed with ImageJ 1.50b (NIH, USA)[55] and Fiji 2.0.0-rc-65[56]. Velocity of cluster (Figs. 3b and 4b) was calculated from the position of centroid of cluster. Velocity of filament (Fig. 5D) was calculated by manually tracking the tip of the filament. Passing count (**Figs. 2b** and **7b**) was visualized using a Temporal-Color Code plugin, while the PIV plugin [59, 60] was used to visualize and analyze cell flow (**Figs. 3e** and **4d**). Flow between first two slices (seconds 0 and 10 in both **Figs. 3e** and **4d**) was calculated in window size 128 px spaced 64 px. The correlation threshold set to 0.6. The statistical computing software, R-3.2.3 (64 bit) (R Core Team, 2016)[59] was used for statistical analysis.

Data Analysis

Colony size distribution (**Figs. 2d–e** and **Figs. 7d–e**) was analyzed using software package poweR-law on R [36], which is based on a method described in [35]. Briefly, we initially fitted the experimental data to the power-law distribution. The estimated power index and the lower cut-off value were set to minimize the Kolmogorov-Smirnov statistic value (*KSd*) of the estimated and the experimental datasets. Then, we performed a goodness-of-fit test. Then, a dataset of composite values was synthesized from the estimated equation. This dataset was prepared so that the ratio of the number of data points above the cut-off value to that below the cut-off value was equivalent to that of the experimental data. For this synthetic dataset, data above the cut-off value were randomly selected to follow the estimated distribution, while data below the cut-off value were randomly sampled from the experimental data below the cut-off value. For each synthetic dataset, the KS value (*KSsim*) was calculated using the same steps as those performed to calculate *KSd*. This process was repeated, following the bootstrapping method, enabling us to determine the probability (*p*) of *KSd* appearing greater than *KSsim*. Clauset et al. [35] have proposed that H_0 (the experimental data follows the power-law distribution) should be rejected if the *p*-value is less than 0.1. To select the model distribution, we performed the Vuong's test, which is a likelihood ratio test for model selection using the Kullback-Leibler criterion [35, 36]. This tests the null hypothesis H_0: both distributions are equally far from the true distribution versus the alternative hypothesis H_1: one of the test distributions is closer to the true distribution. If the *p*-value given by the test is greater than 0.1, then the test is inconclusive, according to Clauset et al. [35]. Velocity and length data shown on **Fig. 5d** and **Fig. S4** were manually measured using ImageJ and calculated with R. The regression line on **Fig. 5d** is based on the data shown in **Fig. S4**. We calculated the slope and R-squared value of the linear regression under each length displayed in the horizontal axis of **Fig. S4.** Although several peaks are shown in **Fig. S4b**, we chose the dataset under 95.98 μm which was determined to be largest number showing peak of adjusted R-squared to perform linear regression.

List of Abbreviations

CDF: cumulative distribution function
EPS: extracellular polysaccharides
JPC: junction pore complex
KS: Kolmogorov-Smirnov (value, statistic)
PDF: probability distribution function
PIV: particle image velocimetry

Declarations

Ethics approval and consent to participate

Not applicable.

Consent for publication

Not applicable.

Availability of data and materials

All the datasets used are available as the Daseset SI file. The strain used in the current study is available from the Microbial Culture Collection at the National Institute for Environmental Studies (NIES collection, Japan) or the corresponding author on reasonable request. Source code for simulation is available at https://github.com/yh1984/Hisamoto_Yamamoto2020.

Competing interests

The authors declare that they have no competing interests.

Funding

This work was supported by Grants-in-Aid from the Japanese Society for Promotion of Sciences (22520150, 25650111, 19K21608 to HI; 23127511 and 25127717 to AT). The funding bodies had no role in the design of the study, collection, analysis, and interpretation of data and in writing the manuscript.

Authors' contributions

HI isolated the strain; HI, AT, and HY conceived and designed the experiments; HY, YF, YS, TK, and HI performed the experiments; AT proposed a basic idea of cluster transition and PIV analysis; SH performed simulation; HY, AT, and HI analyzed the data; HY and HI wrote the manuscript. All authors read and approved the final manuscript.

Acknowledgements

We thank the members of Iwasaki and Takamatsu laboratories and metaPhorest bioaesthetics platform for their valuable discussion and comments on this manuscript, especially Keita Tanaka, Taku Saito and Taku Kimura for sharing preliminary results. We also thank Dr. Yu Hirose (Toyohashi University of Technology) for his help on NIES culture collection.

References

1. Wakita JI, Tsukamoto S, Yamamoto K, Katori M, Yamada Y. Phase diagram of collective motion of bacterial cells in a shallow circular pool. J Phys Soc Japan. 2015;84:1–6.

493 2. Ben-Jacob E, Cohen I, Gutnick DL. Cooperative organization of bacterial colonies: from genotype to
494 morphotype. Annu Rev Microbiol. 1998;52:779–806.
495 3. Ohgiwari M, Matsushita M, Matsuyama T. Morphological changes in growth phenomena of bacterial colony
496 patterns. J Phys Soc Japan. 1992;61:816–22.
497 4. Wakita J, Komatsu K, Nakahara A, Matsuyama T, Matsushita M. Experimental investigation on the validity
498 of population dynamics approach to bacterial colony formation. J Phys Soc Japan. 1994;63:1205–11.
499 5. Ben-Jacob E, Schochet O, Tenenbaum A, Cohen I, Czirók A, Vicsek T. Generic modelling of cooperative
500 growth patterns in bacterial colonies. Nature. 1994;368:46–9.
501 6. Gillert K-E. *Bacillus circulans* (jordan) aufbau und verhalten beweglicher kolonien. Göttingen, Germany:
502 lnsititut fur den Wissenschaftlichen Film; 1975.
503 7. Ingham CJ, Ben-Jacob E. Swarming and complex pattern formation in *Paenibacillus vortex* studied by
504 imaging and tracking cells. BMC Microbiol. 2008;8:36.
505 8. Kobayashi K, Kanesaki Y, Yoshikawa H. Genetic analysis of collective motility of *Paenibacillus* sp.
506 NAIST15-1. PLoS Genet. 2016;12:1–30.
507 9. Gibiansky ML, Hu W, Dahmen KA, Shi W, Wong GCL. Earthquake-like dynamics in *Myxococcus xanthus*
508 social motility. Proc Natl Acad Sci. 2013;110:2330–5.
509 10. Tamulonis C, Kaandorp J. A model of filamentous cyanobacteria leading to reticulate pattern formation.
510 Life. 2014;4:433–56.
511 11. Fujikawa H, Matsushita M. Fractal growth of *Bacillus subtilis* on agar plates. J Phys Soc Japan.
512 1989;58:3875–8.
513 12. Ben-Jacob E, Schochet O, Tenenbaum A, Cohen I, Czirók A, Vicsek T. Generic modelling of cooperative
514 growth patterns in bacterial colonies. Nature. 1994;368:46–9.
515 13. Henriksen SD, Svendsen M. Rotating and wandering colonies in a strain of genus *Bacillus*. Acta Pathol
516 Microbiol Scand. 1946;23:387–93.
517 14. Henrichsen J. Bacterial surface translocation: a survey and a classification. Bacteriol Rev. 1972;36:478–503.
518 15. Finkelshtein A, Roth D, Ben-Jacob E, Ingham CJ. Bacterial swarms recruit cargo bacteria to pave the way in
519 toxic environments. MBio. 2015;6:1–10.
520 16. Fujihara M, Maeda K, Sasamori E, Matsushita M, Harasawa R. Effects of chelating reagents on colonial
521 appearance of *Paenibacillus alvei* isolated from canine oral cavity. 2009.
522 17. O'Connor KA, Zusman DR. Patterns of cellular interactions during fruiting-body formation in *Myxococcus*
523 *xanthus*. J Bacteriol. 1989;171:6013–24.
524 18. Wu Y, Kaiser AD, Jiang Y, Alber MS. Periodic reversal of direction allows myxobacteria to swarm. Proc
525 Natl Acad Sci. 2009;106:1222–7.
526 19. Li Y, Sun H, Ma X, Lu A, Lux R, Zusman D, et al. Extracellular polysaccharides mediate pilus retraction
527 during social motility of *Myxococcus xanthus*. Proc Natl Acad Sci. 2003;100:5443–8.
528 20. Black WP, Xu Q, Yang Z. Type IV pili function upstream of the dif chemotaxis pathway in *Myxococcus*
529 *xanthus* EPS regulation. Mol Microbiol. 2006;61:447–56.
530 21. Balagam R, Igoshin OA. Mechanism for collective cell alignment in *Myxococcus xanthus* bacteria. PLoS

Comput Biol. 2015;11:1–20.
22. Thutupalli S, Sun M, Bunyak F, Palaniappan K, Shaevitz JW. Directional reversals enable *Myxococcus xanthus* cells to produce collective one-dimensional streams during fruiting-body formation. J R Soc Interface. 2015;12:20150049.
23. Shepard RN, Sumner DY. Undirected motility of filamentous cyanobacteria produces reticulate mats. Geobiology. 2010;8:179–90.
24. Richardson L, Stanić D, May A, Brownell A, Gantar M, Campagna S. Ecology and physiology of the pathogenic cyanobacterium *Roseofilum reptotaenium*. Life. 2014;4:968–87.
25. Sato N, Katsumata Y, Sato K, Tajima N. Cellular dynamics drives the emergence of supracellular structure in the cyanobacterium, *Phormidium* sp. KS. Life. 2014;4:819–36.
26. Levy D, Requeijo T. Stochastic models for phototaxis. Bull Math Biol. 2008;70:1684–706.
27. Galante A, Wisen S, Bhaya D, Levy D. Modeling local interactions during the motion of cyanobacteria. J Theor Biol. 2012;309:147–58.
28. Ursell T, Chau RMW, Wisen S, Bhaya D, Huang KC. Motility enhancement through surface modification is sufficient for cyanobacterial community organization during phototaxis. PLoS Comput Biol. 2013;9.
29. Varuni P, Menon SN, Menon GI. Phototaxis as a collective phenomenon in cyanobacterial colonies. Sci Rep. 2017;7:1–10.
30. Castenholz RW. Motility and taxes. In: The Biology of Cyanobacteria. University of California Press; 1982. p. 413–39.
31. Castenholz RW, Rippka R, Herdman M, Wilmotte A. Form- *Pseudanabaena*. In: Boone DR, Castenholz RW, Garrity GM, editors. Bergey's Manual of Systematic Bacteriology Volume One. 2nd edition. New York, NY: Springer New York; 2001. p. 554–7.
32. Wilde A, Mullineaux CW. Motility in cyanobacteria: polysaccharide tracks and type IV pilus motors. Mol Microbiol. 2015;98:998–1001.
33. Brahamsha B, Bhaya D. Motility in unicellular and filamentous cyanobacteria. Cell Biol Cyanobacteria. 2014; September:233–62.
34. Cohen I, Ron IG, Ben-Jacob E. From branching to nebula patterning during colonial development of the *Paenibacillus alvei* bacteria. Phys A Stat Mech its Appl. 2000;286:321–36.
35. Matsuyama T, Matsushita M. Population morphogenesis by cooperative bacteria. Forma. 2001;16:307–26.
36. Janulevicius A, Loosdrecht M Van, Picioreanu C. Short-range guiding can result in the formation of circular aggregates in myxobacteria populations. 2015;:1–17.
37. Burchard RP. Trail following by gliding bacteria. J Bacteriol. 1982;152:495–501.
38. Starruß J, Peruani F, Jakovljevic V, Søgaard-Andersen L, Deutsch A, Bär M. Pattern-formation mechanisms in motility mutants of *myxococcus xanthus*. Interface Focus. 2012;2:774–85.
39. Halfen LN, Castenholz RW. Gliding motility in the blue-green alga *Oscillatoria princeps*. J Phycol. 1971;7:133–45.
40. Adams DG. How do cyanobacteria glide ? Microbiology. 2001;28:131–3.
41. Hoiczyk E, Baumeister W. The junctional pore complex, a prokaryotic secretion organelle, is the molecular

motor underlying gliding motility in cyanobacteria. Curr Biol. 1998;8:1161–8.
42. Duggan PS, Gottardello P, Adams DG. Molecular analysis of genes in *Nostoc punctiforme* involved in pilus biogenesis and plant infection. J Bacteriol. 2007;189:4547–51.
43. Risser DD, Meeks JC. Comparative transcriptomics with a motility-deficient mutant leads to identification of a novel polysaccharide secretion system in *Nostoc punctiforme*. Mol Microbiol. 2013;87:884–93.
44. Risser DD, Chew WG, Meeks JC. Genetic characterization of the hmp locus, a chemotaxis-like gene cluster that regulates hormogonium development and motility in *Nostoc punctiforme*. Mol Microbiol. 2014;92:222–33.
45. Khayatan B, Meeks JC, Risser DD. Evidence that a modified type IV pilus-like system powers gliding motility and polysaccharide secretion in filamentous cyanobacteria. Mol Microbiol. 2015;98:1021–36.
46. Sugi T, Ito H, Nishimura M, Nagai KH. *C. elegans* collectively forms dynamical networks. Nat Commun. 2019;10.
47. Sumino Y, Nagai KH, Shitaka Y, Tanaka D, Yoshikawa K, Chaté H, et al. Large-scale vortex lattice emerging from collectively moving microtubules. Nature. 2012;483:448–52.
48. Nagai KH, Sumino Y, Montagne R, Aranson IS, Chaté H. Collective motion of self-propelled particles with memory. Phys Rev Lett. 2015.
49. Rippka R, Deruelles J, Waterbury JB, Herdman M, Stanier RY. Generic assignments, strain histories and properties of pure cultures of cyanobacteria. Microbiology. 1979;111:1–61.
50. Cole JR, Wang Q, Fish JA, Chai B, McGarrell DM, Sun Y, et al. Ribosomal database project: data and tools for high throughput rrna analysis. Nucleic Acids Res. 2014.
51. Camacho C, Coulouris G, Avagyan V, Ma N, Papadopoulos J, Bealer K, et al. BLAST+: architecture and applications. BMC Bioinformatics. 2009.
52. Edgar RC. MUSCLE: multiple sequence alignment with high accuracy and high throughput. Nucleic Acids Res. 2004;32:1792–7.
53. Larkin MA, Blackshields G, Brown NP, Chenna R, McGettigan PA, McWilliam H, et al. Clustal w and clustal x version 2.0. Bioinformatics. 2007;23:2947–8.
54. Han M V., Zmasek CM. PhyloXML: XML for evolutionary biology and comparative genomics. BMC Bioinformatics. 2009;10:1–6.
55. Schneider CA, Rasband WS, Eliceiri KW. NIH image to imagej: 25 years of image analysis. Nat Methods. 2012;9:671–5.
56. Schindelin J, Arganda-Carreras I, Frise E, Kaynig V, Longair M, Pietzsch T, et al. Fiji: an open-source platform for biological-image analysis. Nat Methods. 2012;9:676–82.
57. Tseng Q, Duchemin-Pelletier E, Deshiere A, Balland M, Guilloud H, Filhol O, et al. Spatial organization of the extracellular matrix regulates cell-cell junction positioning. Proc Natl Acad Sci U S A. 2012;109:1506–11.
58. Tseng Q. Study of multicellular architecture with controlled microenvironment. Lab Chip. 2011.
59. Ihaka R, Gentleman R. R: a language for data analysis and graphics. J Comput Graph Stat. 1996.

Figure Legends

Figure 1. Morphology of *Pseudanabaena* sp. NIES-4403. a. Light microscopic image of cell morphology. **b**. Scanning electron microscope image of cell morphology. **c**. Transmission electron microscopy image. **d**. Colonies on solid BG-11 medium (90-mm plate) 12 days after inoculation at the center of the plate.

Figure 2. Scattered colony pattern of *Pseudanabaena* sp. NIES-4403 on solid BG-11 media. a. Time-lapse images of *Pseudanabaena* on a 90-mm plate. Hour 0 represents time that time-lapse photography started, corresponding to ~10 hours after inoculating a cell suspension at the center of the plate. Time-lapse imaging was performed every hour, and the images were compiled into **Movies S1**. **b**. Trajectory of wandering colonies over 120 h from hour 0 of **Movie S1**. Color represents the passing count (log) (1 count, cyan; 120 count, magenta). **c**. A kymograph of colonies represented by yellow lines shown in **panel a** over a 200-h period (top, hour 0; bottom, hour 200). Cyan and magenta triangles represent a rotating disk and a comet-like wandering cluster, respectively**. d.** Colony size distribution at hours 100 and 200 on a log-log plot. **e.** Cumulative distribution function of colony size at hours 100 and 200. It should be noted that the largest cluster located at the center is not considered because it is derived from the initial spot of inoculation; thus, its morphological pattern is due to both autonomous behavior and the artificial inoculation setting.

Figure 3. Comet-like wandering cluster displaying coordination in the direction of movement and velocity. a. Trajectory of a representative comet-like wandering cluster. Colors indicate the positions of the cluster in between hours 70 (cyan) and 200 (magenta). For more details, see **Movie S2**, which was extracted from **Movie S1**. **b**. Time course of changes in velocity and size of the cluster shown in panel **a**. Color bar on the horizontal axis is the same as shown in **panel a**. Arrowheads show the time when the velocity accelerated transiently. **c**. Trajectory of the same cluster during the first spike in velocity that peaked at hour 154 (Green). Orange represents trajectories of three other preceding clusters. It should be noted that the velocity of the cluster shown in cyan started to increase at hour 152 (**panel b**), when the cluster passed over a trail of a preceding cluster. From this time up to hour 156, the cluster passed over two other trails. **d**. Movement and morphology of a comet-like cluster wandering for 10 min. The video is provided as **Movie S3**. **e**. PIV analysis of the movement of the comet-like cluster with confocal images of autofluorescing cells. Color bars and arrows indicate trajectories of single cells within a period of 10 min (cyan to magenta) and the result of PIV analysis (velocity), respectively. The video is shown in **Movie S4**. **f**. U-shaped motion of a single filament.

Figure 4. Rotating disk clusters. a. Trajectory of a cluster turning from a comet-like cluster to a rotating disk. Colors indicate the positions of the cluster at hours 21 (cyan) and 60 (magenta). Photographs show only the colony profile at hour 60, and the arrowhead indicates the resulting rotating disk. For more details, see **Movie S5**, which was extracted from **Movie S1**. **b.** Time course of changes in

velocity and size of the cluster shown in **panel a**. Color bar on the horizontal axis is the same as shown in **panel a**. **c.** Movement and morphology of a rotating disk cluster within a period of 10 min. The video is provided in **Movie S2**. **d**. PIV analysis of the movement of the rotating disk cluster with confocal images of autofluorescing cells. Color bars and arrows indicate trajectories of single cells within a period of 10 min (cyan to magenta) and the result of PIV analysis (velocity), respectively. The video is provided in **Movie S6**. **e.** Correlation between the distance from the center of the rotating disk and the magnitude (velocity) of the PIV analysis. Detailed spatial distribution is shown in **Fig. S2**.

Figure 5. Trail following and nematic alignment (bundle formation) of filaments. a. Microscopic view of bundled filaments. Colors indicate the trajectory of the tip positions of each filament (0 sec in cyan to 120 sec in magenta). The video is provided in **Movie S7**. **b.** A filament following a trail shown as a thin line before the filament. Points indicate positions of the tip at each time point shown by color (0 min in cyan, 40 min in magenta). The video is provided in **Movie S8**. **c.** Time-lapse images of colliding filaments. Points indicate the trajectory of tip positions shown by color (0 min in cyan, 12 min in magenta). The video is provided in **Movie S9**. **d.** Relationship between the velocity and length of single filaments. Line indicates the result of regression analysis performed on data with values less than 95.98 μm (for details, see text and **Fig. S4**).

Figure 6. Development of comet and disk clusters from a single or a bundle of filaments. a-f. Schematic representation of the transition of colony patterns. Bacterial filaments and possibly secreted mucilage are shown in brown and pale blue, respectively. Spontaneous bending of a protruding filament in a bundle (**a**, upper) or collision of two single filaments crossing paths (**a**, bottom) leads to the formation of a "top covered" bundle (**b**) which is a precursor to a comet-like wandering cluster. Collision of comets (**c**) and propagation of cells enlarge the size of comet-like clusters (**d**). Change in the direction of the movement (**e**) can spontaneously lead to a self-following orbit, which develops into a rotating disk (**f**). Detachment of filaments and collision-based decay of the clusters also occur, leading to transitions from larger clusters to smaller clusters, bundle, or filaments. **g-i.** Time-lapse images of transitioning *Pseudanabaena* cluster patterns. **g.** Enlargement of comet-like cluster by collision of two comets. The video is provided in **Movie S10**. **h.** Transition from come-like wandering cluster to self-following orbit, developing into a rotating disk. The video is provided in **Movie S11**. **i**. Collision of a comet-like cluster (moving from the upper right to the center) to a rotating disk (center), leading to the collapse of the disk and reversion to a comet-like cluster. The video is provided in **Movie S12**.

Figure 7. A simple self-propelled particle model reproducing the scattered colony pattern. The organization of the panels in this figure (simulations) is the same as that of **Fig. 2** (experimental data). **a**. Simulation of scattered (discrete) colony pattern formation. For details, see **Movie S13**. **b.** Trajectory of wandering agents over 2000 steps from time 0 of **Movie S13**. Colors represent the passing count (log) (1 count, cyan; 337 counts, magenta). **c**. A kymograph of agents on yellow lines in **panel a** over 2000 steps

683 (top, step 1; bottom, step 2000). **d.** Colony size distribution of the model at steps 1000 and 2000 of **Movie**
684 **S13**. **e.** Cumulative distribution function of the aggregation size of the model at steps 1000 and 2000.
685
686

687 **Table 1.** Parameters and values of the model. Particle number, 500; maximum step, 2000. Initial position
688 was set to 0 < x < 2 and 0 < y < 2.

Mean velocity	v_0	0.1
Length of filament	l	1.0
Range of repulsive force	r^r	0.2
Mean rotation rate	ω_0	0.0005
Standard deviation of rotation rate	σ_ω	0.2
Correlation time of rotation rate	τ	500
Coefficient of repulsive force	k^r	10
Coefficient of attractive force	k^a	0.1

689
690

Additional Files (Supplementary information)

Additional file 1:

Figure S1. Phylogenetic analysis based on the 16S RNA gene. 16S rRNA gene sequence of *Pseudanabaena* NIES-4403 was compared to those deposited with the Ribosomal Database Project (RDP), including 24 closely related sequences chosen according to BLAST search results and 5 representative cyanobacterial strains. Numbers on the junctions represent bootstrap values.

Additional file 2:

Figure S2. Spatial distribution of the velocity of filaments in a rotating disk by PIV analysis. Colors of points show magnitudes of PIV (blue, minimal value of 0; red, maximal value of 0.1364566). White circles show standard distances from the center position.

Additional file 3:

Figure S3. Staining EPS around cells with Alcian blue. Extracellular polysaccharide was visualized using Alcian blue. Arrowheads indicate the staining of EPS around filaments in some aggregates.

Additional file 4:

Figure S4. Regression analysis on the filament length and moving velocity. The regression line shown in **Figure 5D** is based on the slope (**a**) and correlation index (adjusted R-squared value) of (**b**) regression curves when the upper threshold of the filament length is changed. We considered the area from 0 to 100 μm, because this area provided relatively higher correlation indices.

Additional file 5:

Movie S1. Time-lapse images of *Pseudanabaena* sp. NIES-4403 on a 90-mm agar plate. Cells were inoculated at the center and incubated for about one day before recording the video. Colors indicate the position of the cluster shown in **Figs. 3a** and **4a**. For details, see Materials and Methods.

Additional file 6:

Movie S2. Time-lapse images of comet-like wandering cluster (extracted from **Movie S1**).

Additional file 7:

Movie S3. Time-lapse images of wandering or rotating clusters on agar-containing media. A comet-like wandering cluster (upper left) and a rotating disk (lower right) are visible. Some bundled filaments and single filaments are also visible.

Additional file 8:

Movie S4. Time-lapse confocal images of a comet-like wandering cluster.

Additional file 9:

Movie S5. Time-lapse images of rotating disk (extracted from **Movie S1**).

Additional file 10:

Movie S6. Time-lapse confocal images of a rotating disk.

Additional file 11:

Movie S7. Time-lapse images of a bundle composed of aligned filaments. The bundle visible at the beginning of this movie consists of nine filaments.

Additional file 12:

Movie S8. Time-lapse of images of a single filament following a trail.

Additional file 13:

Movie S9. Collision between two filament, moving parallel to each other.

Additional file 14:

Movie S10. Collision between two comet-like clusters, forming a unified cluster.

Additional file 15:

Movie S11. Transition from a comet-like cluster to a rotating cluster.

Additional file 16:

Movie S12. Collision between a comet-like cluster and a rotating disk, leading to the collapse of the rotating disk.

Additional file 17:

Movie S13. Video of the simulated result of the self-propelled particle model.

Additional file 18:

Dataset S1. Original dataset used for figures are compiled.

Figures

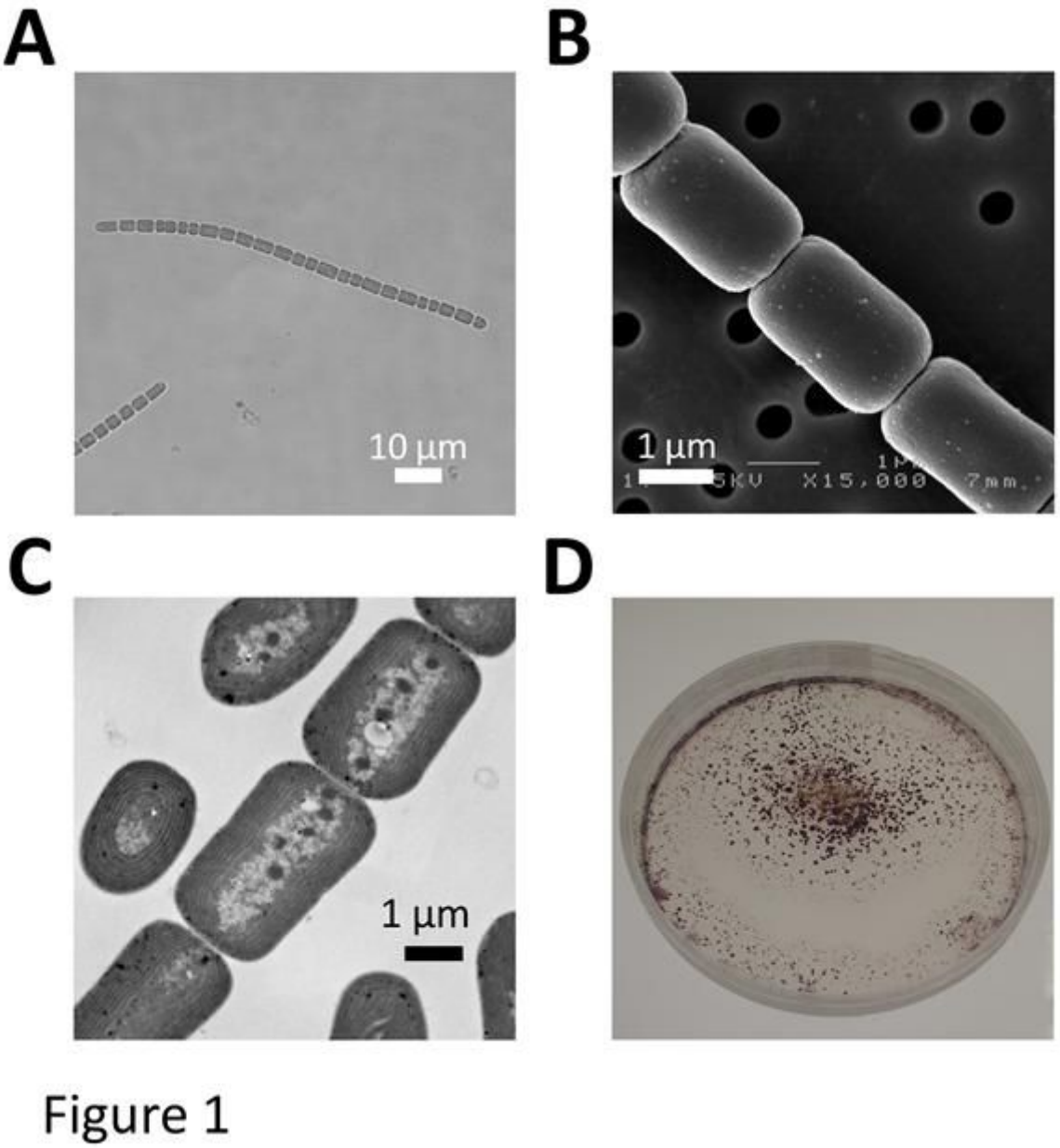

Figure 1

Figure 1

Morphology of Pseudanabaena sp. NIES-4403. a. Light microscopic image of cell morphology. b. Scanning electron microscope image of cell morphology. c. Transmission electron microscopy image. d. Colonies on solid BG-11 medium (90-mm plate) 12 days after inoculation at the center of the plate.

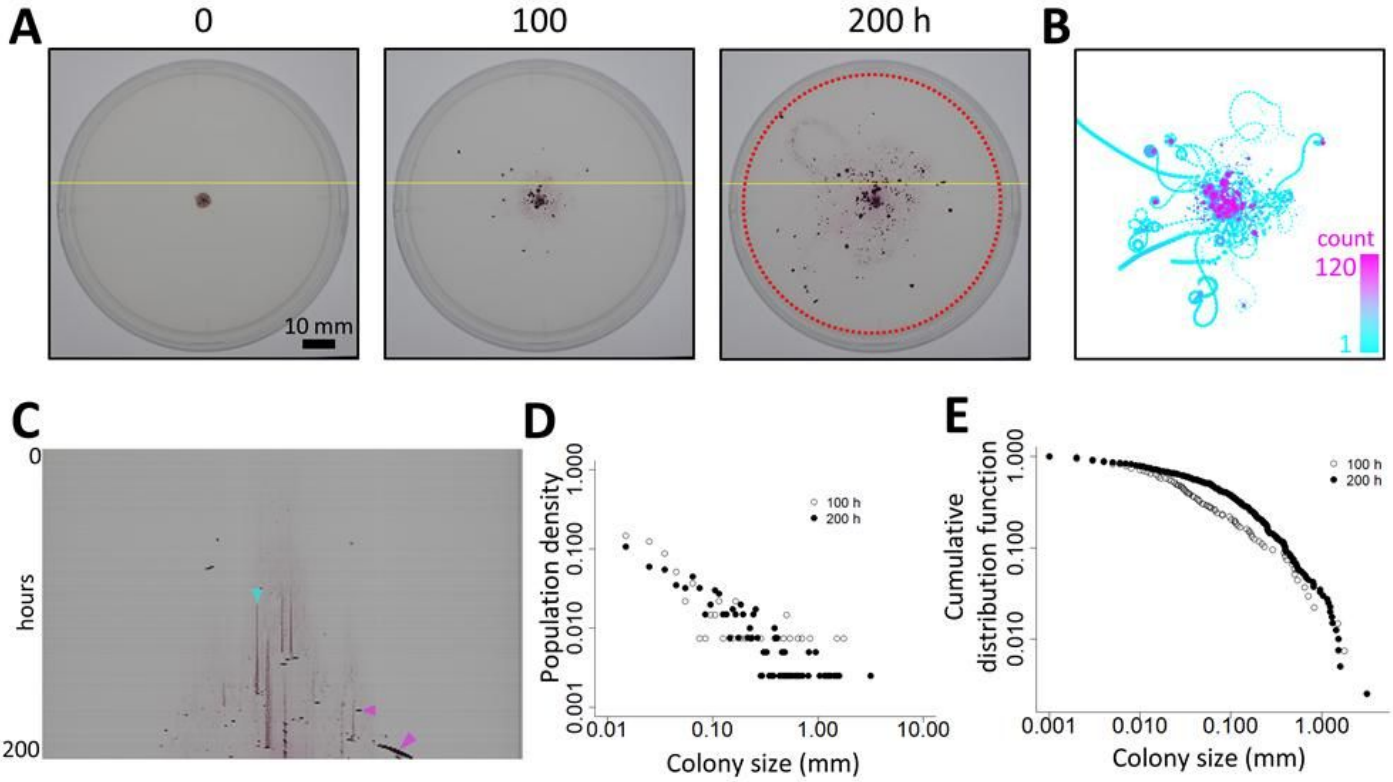

Figure 2

Figure 2

Scattered colony pattern of Pseudanabaena sp. NIES-4403 on solid BG-11 media. a. Time-lapse images of Pseudanabaena on a 90-mm plate. Hour 0 represents time that time-lapse photography started, corresponding to ~10 hours after inoculating a cell suspension at the center of the plate. Time-lapse imaging was performed every hour, and the images were compiled into Movies S1. b. Trajectory of wandering colonies over 120 h from hour 0 of Movie S1. Color represents the passing count (log) (1 count, cyan; 120 count, magenta). c. A kymograph of colonies represented by yellow lines shown in panel a over a 200-h period (top, hour 0; bottom, hour 200). Cyan and magenta triangles represent a rotating disk and a comet-like wandering cluster, respectively. d. Colony size distribution at hours 100 and 200 on a log-log plot. e. Cumulative distribution function of colony size at hours 100 and 200. It should be noted that the largest cluster located at the center is not considered because it is derived from the initial spot of inoculation; thus, its morphological pattern is due to both autonomous behavior and the artificial inoculation setting.

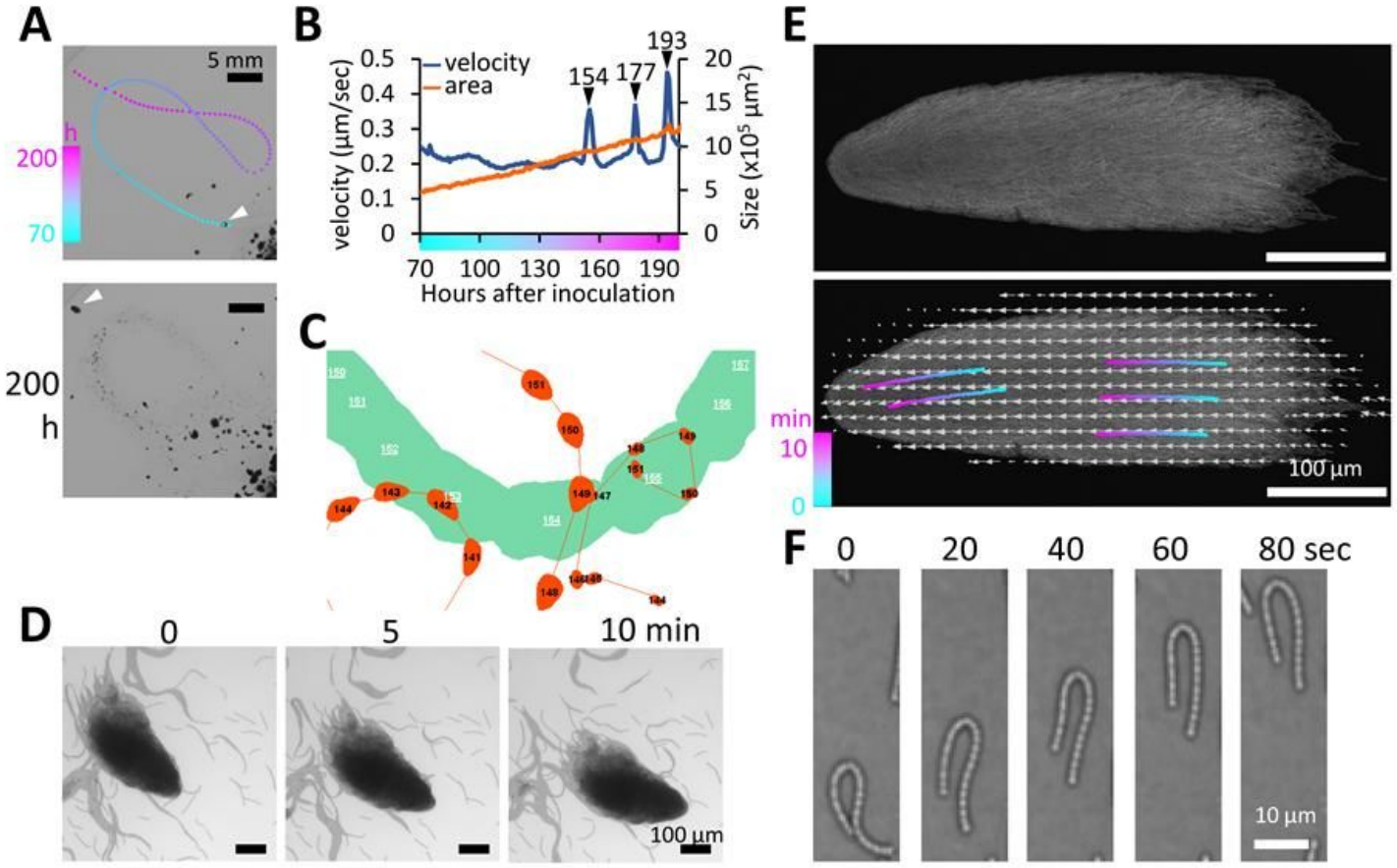

Figure 3

Figure 3

Comet-like wandering cluster displaying coordination in the direction of movement and velocity. a. Trajectory of a representative comet-like wandering cluster. Colors indicate the positions of the cluster in between hours 70 (cyan) and 200 (magenta). For more details, see Movie S2, which was extracted from Movie S1. b. Time course of changes in velocity and size of the cluster shown in panel a. Color bar on the horizontal axis is the same as shown in panel a. Arrowheads show the time when the velocity accelerated transiently. c. Trajectory of the same cluster during the first spike in velocity that peaked at hour 154 (Green). Orange represents trajectories of three other preceding clusters. It should be noted that the velocity of the cluster shown in cyan started to increase at hour 152 (panel b), when the cluster passed over a trail of a preceding cluster. From this time up to hour 156, the cluster passed over two other trails. d. Movement and morphology of a comet-like cluster wandering for 10 min. The video is provided as Movie S3. e. PIV analysis of the movement of the comet-like cluster with confocal images of autofluorescing cells. Color bars and arrows indicate trajectories of single cells within a period of 10 min (cyan to magenta) and the result of PIV analysis (velocity), respectively. The video is shown in Movie S4. f. U-shaped motion of a single filament.

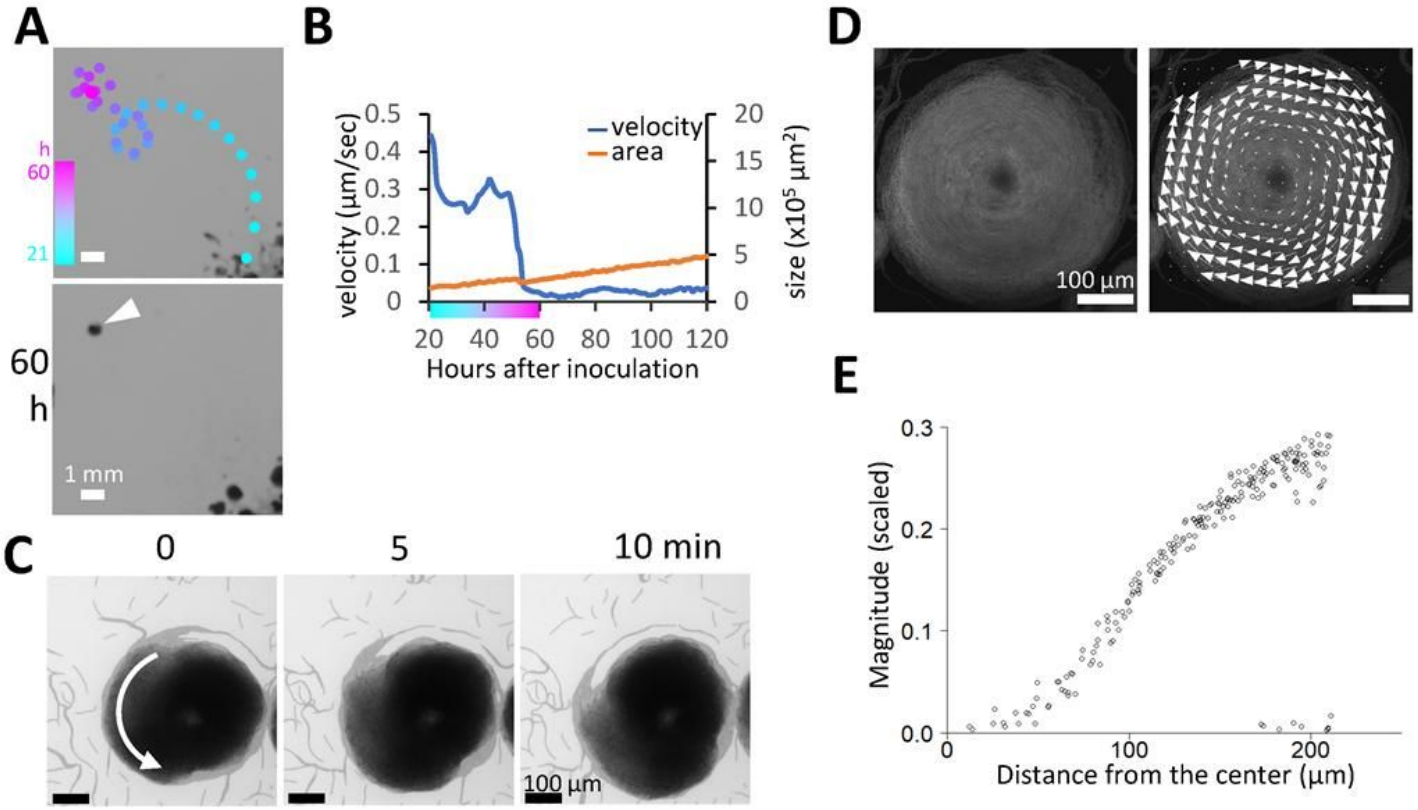

Figure 4

Figure 4

Rotating disk clusters. a. Trajectory of a cluster turning from a comet-like cluster to a rotating disk. Colors indicate the positions of the cluster at hours 21 (cyan) and 60 (magenta). Photographs show only the colony profile at hour 60, and the arrowhead indicates the resulting rotating disk. For more details, see Movie S5, which was extracted from Movie S1. b. Time course of changes in velocity and size of the cluster shown in panel a. Color bar on the horizontal axis is the same as shown in panel a. c. Movement and morphology of a rotating disk cluster within a period of 10 min. The video is provided in Movie S2. d. PIV analysis of the movement of the rotating disk cluster with confocal images of autofluorescing cells. Color bars and arrows indicate trajectories of single cells within a period of 10 min (cyan to magenta) and the result of PIV analysis (velocity), respectively. The video is provided in Movie S6. e. Correlation between the distance from the center of the rotating disk and the magnitude (velocity) of the PIV analysis. Detailed spatial distribution is shown in Fig. S2.

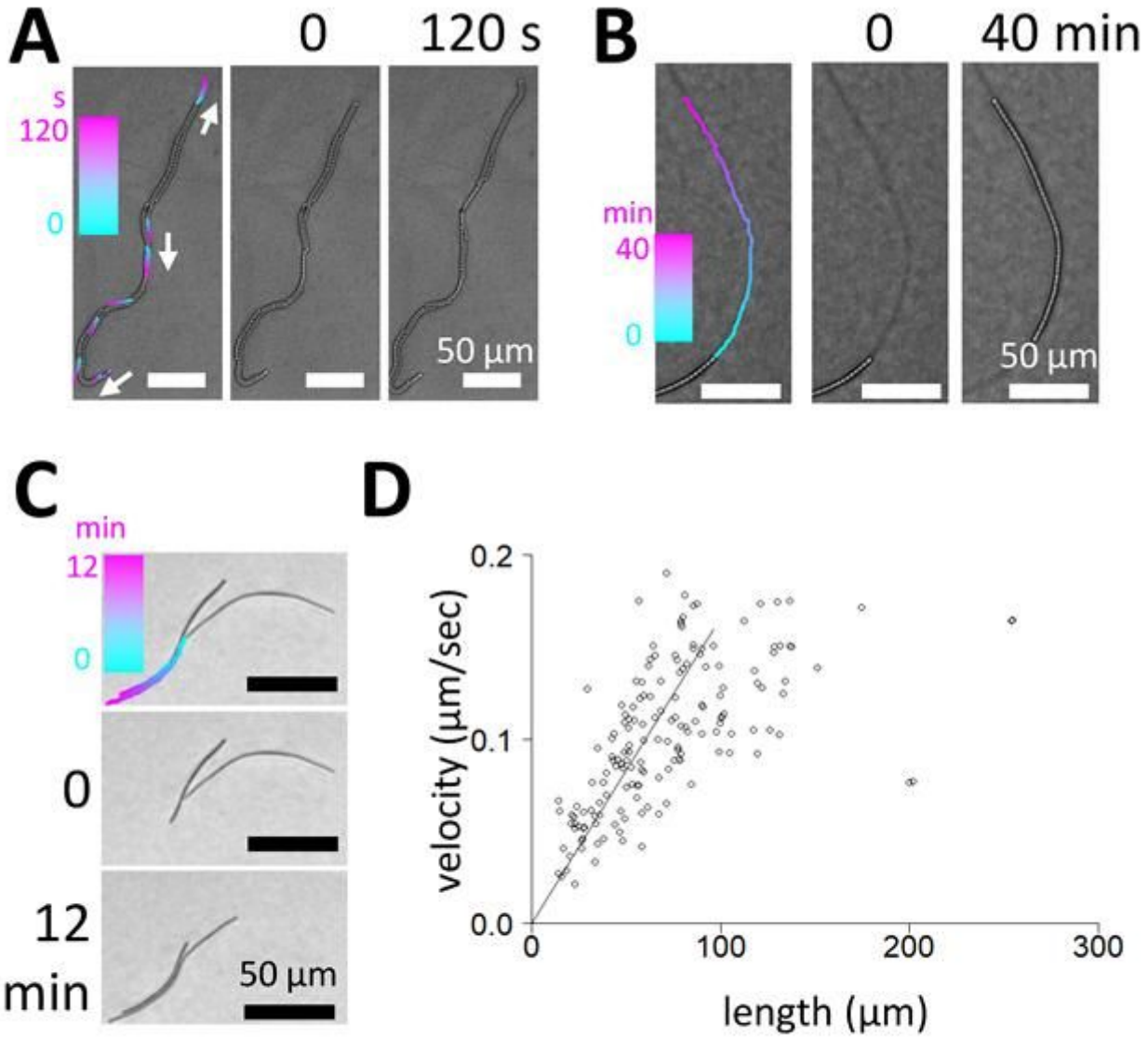

Figure 5

Figure 5

Trail following and nematic alignment (bundle formation) of filaments. a. Microscopic view of bundled filaments. Colors indicate the trajectory of the tip positions of each filament (0 sec in cyan to 120 sec in magenta). The video is provided in Movie S7. b. A filament following a trail shown as a thin line before the filament. Points indicate positions of the tip at each time point shown by color (0 min in cyan, 40 min in magenta). The video is provided in Movie S8. c. Time-lapse images of colliding filaments. Points indicate the trajectory of tip positions shown by color (0 min in cyan, 12 min in magenta). The video is provided in Movie S9. d. Relationship between the velocity and length of single filaments. Line indicates the result of regression analysis performed on data with values less than 95.98 µm (for details, see text and Fig. S4).

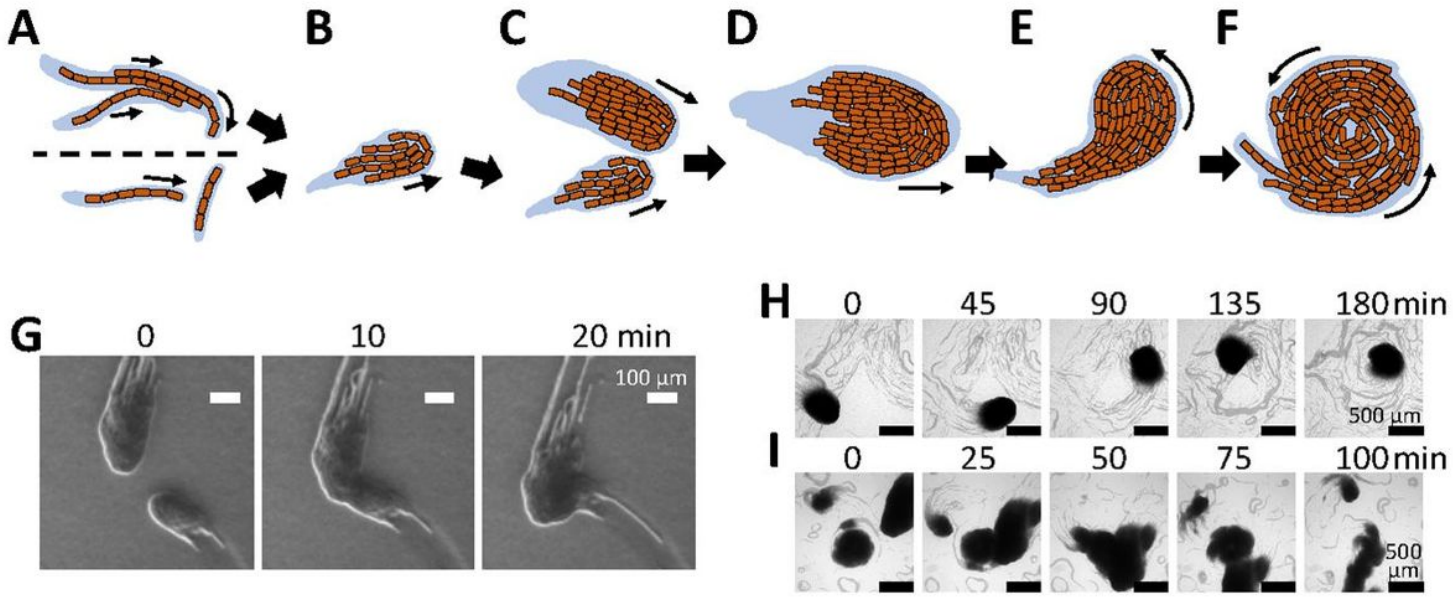

Figure.6

Figure 6

Development of comet and disk clusters from a single or a bundle of filaments. a-f. Schematic representation of the transition of colony patterns. Bacterial filaments and possibly secreted mucilage are shown in brown and pale blue, respectively. Spontaneous bending of a protruding filament in a bundle (a, upper) or collision of two single filaments crossing paths (a, bottom) leads to the formation of a “top covered” bundle (b) which is a precursor to a comet-like wandering cluster. Collision of comets (c) and propagation of cells enlarge the size of comet-like clusters (d). Change in the direction of the movement (e) can spontaneously lead to a self-following orbit, which develops into a rotating disk (f). Detachment of filaments and collision-based decay of the clusters also occur, leading to transitions from larger clusters to smaller clusters, bundle, or filaments. g-i. Time-lapse images of transitioning Pseudanabaena cluster patterns. g. Enlargement of comet-like cluster by collision of two comets. The video is provided in Movie S10. h. Transition from come-like wandering cluster to self-following orbit, developing into a rotating disk. The video is provided in Movie S11. i. Collision of a comet-like cluster (moving from the upper right to the center) to a rotating disk (center), leading to the collapse of the disk and reversion to a comet-like cluster. The video is provided in Movie S12.

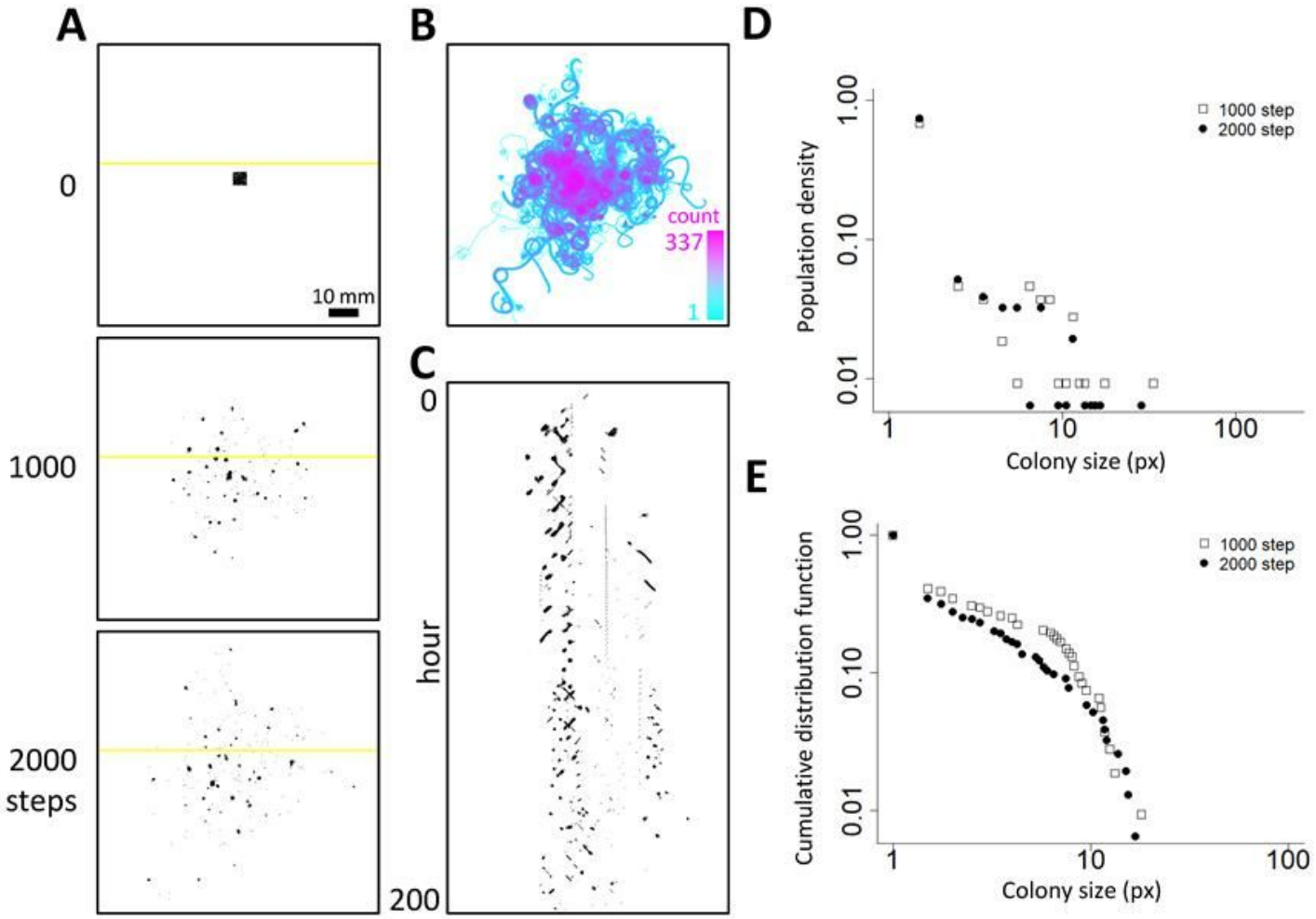

Figure 7

Figure 7

A simple self-propelled particle model reproducing the scattered colony pattern. The organization of the panels in this figure (simulations) is the same as that of Fig. 2 (experimental data). a. Simulation of scattered (discrete) colony pattern formation. For details, see Movie S13. b. Trajectory of wandering agents over 2000 steps from time 0 of Movie S13. Colors represent the passing count (log) (1 count, cyan; 337 counts, magenta). c. A kymograph of agents on yellow lines in panel a over 2000 steps (top, step 1; bottom, step 2000). d. Colony size distribution of the model at steps 1000 and 2000 of Movie S13. e. Cumulative distribution function of the aggregation size of the model at steps 1000 and 2000.

Supplementary Files

This is a list of supplementary files associated with this preprint. Click to download.

- DatasetS1.xlsx
- MovieS13.mp4

- MovieS12.mp4
- MovieS11.mp4
- MovieS10.mp4
- MovieS9.mp4
- MovieS8.mp4
- MovieS7.mp4
- MovieS6.mp4
- MovieS5.mp4
- MovieS4.mp4
- MovieS3.mp4
- MovieS2.mp4
- MovieS1.mp4
- FigureS4.pdf
- FigureS3.pdf
- FigureS2.pdf
- FigureS1.pdf